The Astrophysical Journal, 859:25 (12pp), 2018 May 20 https://doi.org/10.3847/1538-4357/aabc0e

Unambiguous Evidence of Coronal Implosions during Solar Eruptions and Flares

Juntao Wang, P. J. A. Simões, and L. Fletcher
SUPA, School of Physics and Astronomy, University of Glasgow, Glasgow G12 8QQ, UK; j.wang.4@research.gla.ac.uk
Received 2018 January 8; revised 2018 March 29; accepted 2018 April 2; published 2018 May 18

Abstract

In the implosion conjecture, coronal loops contract as the result of magnetic energy release in solar eruptions and flares. However, after almost two decades, observations of this phenomenon are still rare and most previous reports are plagued by projection effects so that loop contraction could be either true implosion or just a change in loop inclination. In this paper, to demonstrate the reality of loop contractions in the global coronal dynamics, we present four events with the continuously contracting loops in an almost edge-on geometry from the perspective of *SDO*/AIA, which are free from the ambiguity caused by the projection effects, also supplemented by contemporary observations from *STEREO* for examination. In the wider context of observations, simulations and theories, we argue that the implosion conjecture is valid in interpreting these events. Furthermore, distinct properties of the events allow us to identify two physical categories of implosion. One type demonstrates a rapid contraction at the beginning of the flare impulsive phase, as magnetic free energy is removed rapidly by a filament eruption. The other type, which has no visible eruption, shows a continuous loop shrinkage during the entire flare impulsive phase, which we suggest shows the ongoing conversion of magnetic free energy in a coronal volume. Corresponding scenarios are described that can provide reasonable explanations for the observations. We also point out that implosions may be suppressed in cases when a heavily mass-loaded filament is involved, possibly serving as an alternative account for their observational rarity.

Key words: Sun: coronal mass ejections (CMEs) – Sun: filaments, prominences – Sun: flares – Sun: magnetic fields – Sun: UV radiation

Supporting material: animations

1. Introduction

Solar eruptions and flares are two main manifestations of magnetic energy release in the corona of the Sun. Hudson (2000) conjectured that a new phenomenon termed "implosion" would accompany these energy release processes, based on the assumption of the dominance of Lorentz force in the coronal dynamics, and the equivalence of magnetic energy and magnetic pressure. The conjecture reads, "During a transient, the coronal field lines must contract in such a way as to reduce $\int_V (B^2/8\pi)dV$." Though it was proposed almost two decades ago, observations of such field implosion phenomena are still rare, compared to numerous eruptions and flares observed.

Remarkable coronal loop contractions in extreme ultraviolet at the periphery of active regions, with speeds of tens to hundreds of km s^{-1}, were reported in a few events ranging from *Geostationary Operational Environmental Satellite* (*GOES*) class B to X (Liu & Wang 2009, 2010; Gosain 2012; Liu et al. 2012; Sun et al. 2012; Simões et al. 2013; Yan et al. 2013; Kushwaha et al. 2015; Wang et al. 2016). As these peripheral loop contractions were always observed face-on and accompanied by eruptions from central magnetic structures (like a filament or an arcade eruption), the possibility could not be ruled out that apparent contraction is a projection effect due to the inclination of the loop plane pushed by the erupting structure, rather than a real contraction (from our survey experience, loop inclining is indeed more commonly observed when the loops are viewed with an edge-on state at the solar limb, and even some of them do not restore back to their original locations). As far as we know, only Petrie (2016) reported edge-on loop contractions in two active regions from the perspective of the *Solar TErrestrial RElations Observatory* (*STEREO*) in 195 Å, but due to the short interval of the process and the long cadence (∼5 minutes), the dynamics was not persistently revealed and not clear enough to be well studied. In addition, both the Petrie (2016) events show dramatic eruptions, but in this paper we also show a new type of loop contraction observed edge-on without violent eruptions. The argument that the contracting loops do not restore to their original positions after the eruptions (Gosain 2012; Liu et al. 2012; Simões et al. 2013; Wang et al. 2016) and evidence from NLFFF extrapolations (Wang et al. 2016) have been used to try to substantiate the reality of the contracting motion, but the doubt that it could be a projection effect can still not be completely excluded, and the ambiguity remains.

In some of the events above, dramatic oscillations were noticed during or after the loop contractions (Liu & Wang 2010; Gosain 2012; Liu et al. 2012; Sun et al. 2012; Simões et al. 2013). Russell et al. (2015) considered a one-loop system as a harmonic oscillator, showing that the contracting and oscillating behaviors can be reproduced by the change in loop equilibrium position due to magnetic energy release underneath, in agreement with the implosion conjecture. Pascoe et al. (2017) included a displacement term for the changing equilibrium position from Russell et al. (2015) for coronal seismology analysis, and only the fundamental kink mode exists associated with the loop contraction in Simões et al. (2013). Liu & Wang (2010) suggested that the interaction between the contracting loops and surrounding ones may also

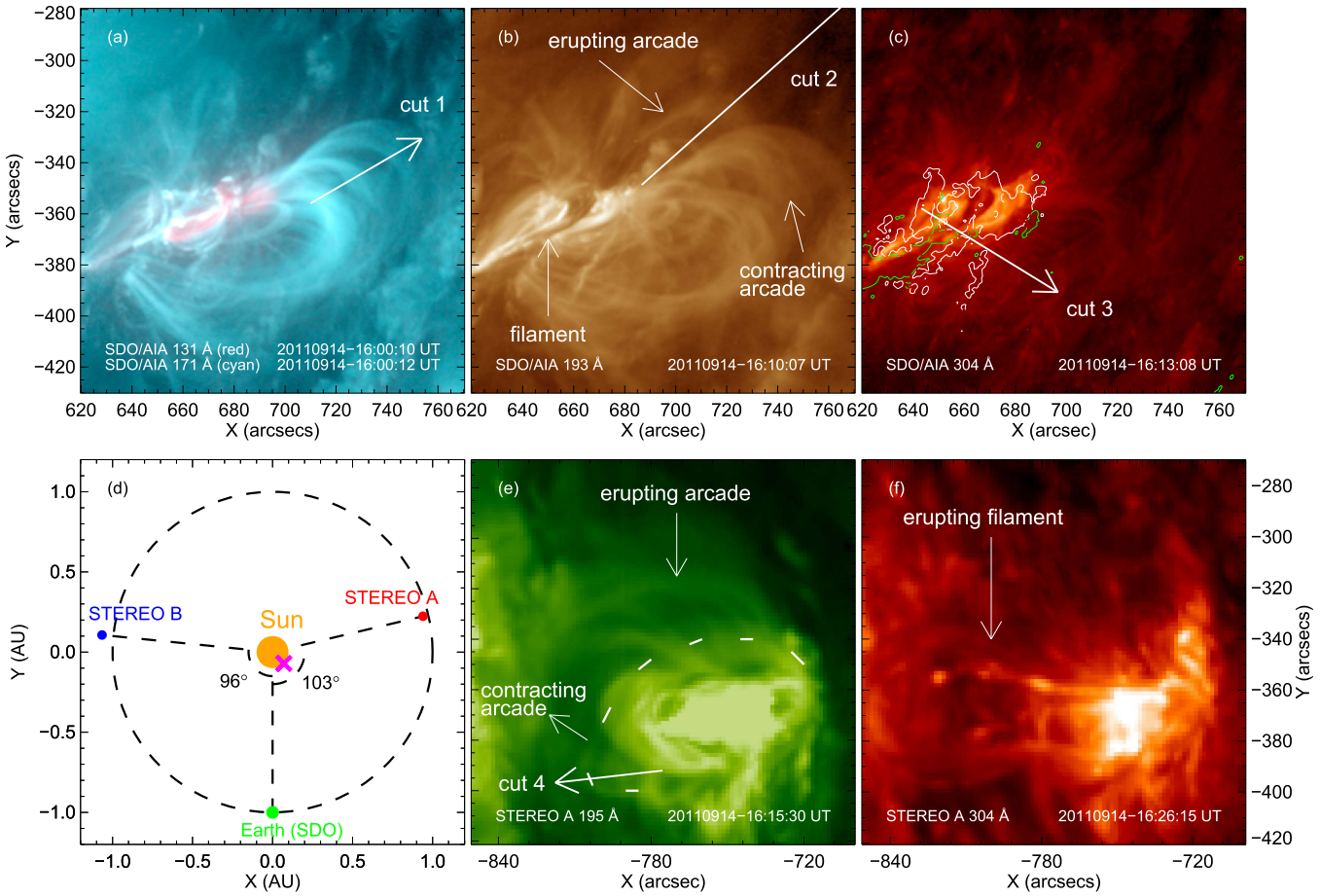

Figure 1. Images for Event I: SOL2011-09-14T16:26. (a)–(c) Observed from the perspective of AIA; 131 Å is red, and 171 Å is cyan in (a) (hereafter for composite images, cyan always represents a low temperature band, like 171 or 193 Å, and the hot 131 Å is always set to red). (d) Relative positions of *SDO* and *STEREO*. The magenta cross shows the longitudinal position of the event. (e)–(f) Observed from the perspective of *STEREO A*. The dashed line in (e) illustrates the location and shape of the contracting arcade. Cuts 1–4 are used for the timeslices in Figure 2. The arrowhead of cut 2 is beyond the image edge. The animation compares panels (a), (b), (e), and (f) for Event I from 2011 September 14 16:00 to 17:00 UT.

(An animation of this figure is available.)

make them oscillate. The model of an isolated simple harmonic oscillator cannot properly describe the dynamics of a continuum medium, where many magnetic strands will interact with each other if not in phase, so a full magnetohydrodynamic (MHD) treatment may be needed for a more accurate description of the dynamics.

A longitudinal field decrease or horizontal field enhancement near the polarity inversion line in the photospheric magnetograms has been detected during many events, especially eruptive flares (Sudol & Harvey 2005; Petrie & Sudol 2010; Wang & Liu 2010; Gosain 2012; Petrie 2012; Sun et al. 2012, 2017). The phenomenon is often explained by the authors exploiting the implosion conjecture, because this predicts a more horizontal field as loops contract, which could probably propagate from the restructuring corona down to the photosphere during the impulsive phase (Hudson et al. 2008; Fisher et al. 2012). However, the non-eruptive X3.1 flare in the famous active region 12192 did not show significant changes in its photospheric horizontal field (Sun et al. 2015; Jiang et al. 2016).

In several MHD simulations with a configuration in which a flux rope is anchored below a magnetic arcade, when the flux rope erupts outward, it can be seen that some of the peripheral unopened arcade field finally contracts[1] toward the central erupting structure, leading to a shorter length compared to its pre-eruption state (Aulanier et al. 2005; Gibson & Fan 2006; Fan & Gibson 2007; Rachmeler et al. 2009; Dudík et al. 2017; Zuccarello et al. 2017). However, Zuccarello et al. (2017) and Dudík et al. (2017) proposed an alternative explanation of the loop contraction in their simulation, using the analogy of vortices in the hydrodynamic situation (further discussed in Section 3.3). Sarkar et al. (2017) recently carried out the first simulation focused on implosions, and found that oscillations of both kink and sausage modes can exist when the loops contract, and that loops in different plasma β regimes may exhibit different dynamic behaviors.

In this paper, we will present direct evidence of continuous implosion phenomena, with the observations shown in Section 2. Based on the main observational properties, Section 3 will demonstrate the validity of the implosion conjecture and categorize the observed implosions into two types, with corresponding models proposed. Conclusions are summarized in Section 4.

[1] Depending on the location of the arcade field, the field would expand, incline and contract, or incline and contract, or directly contract.

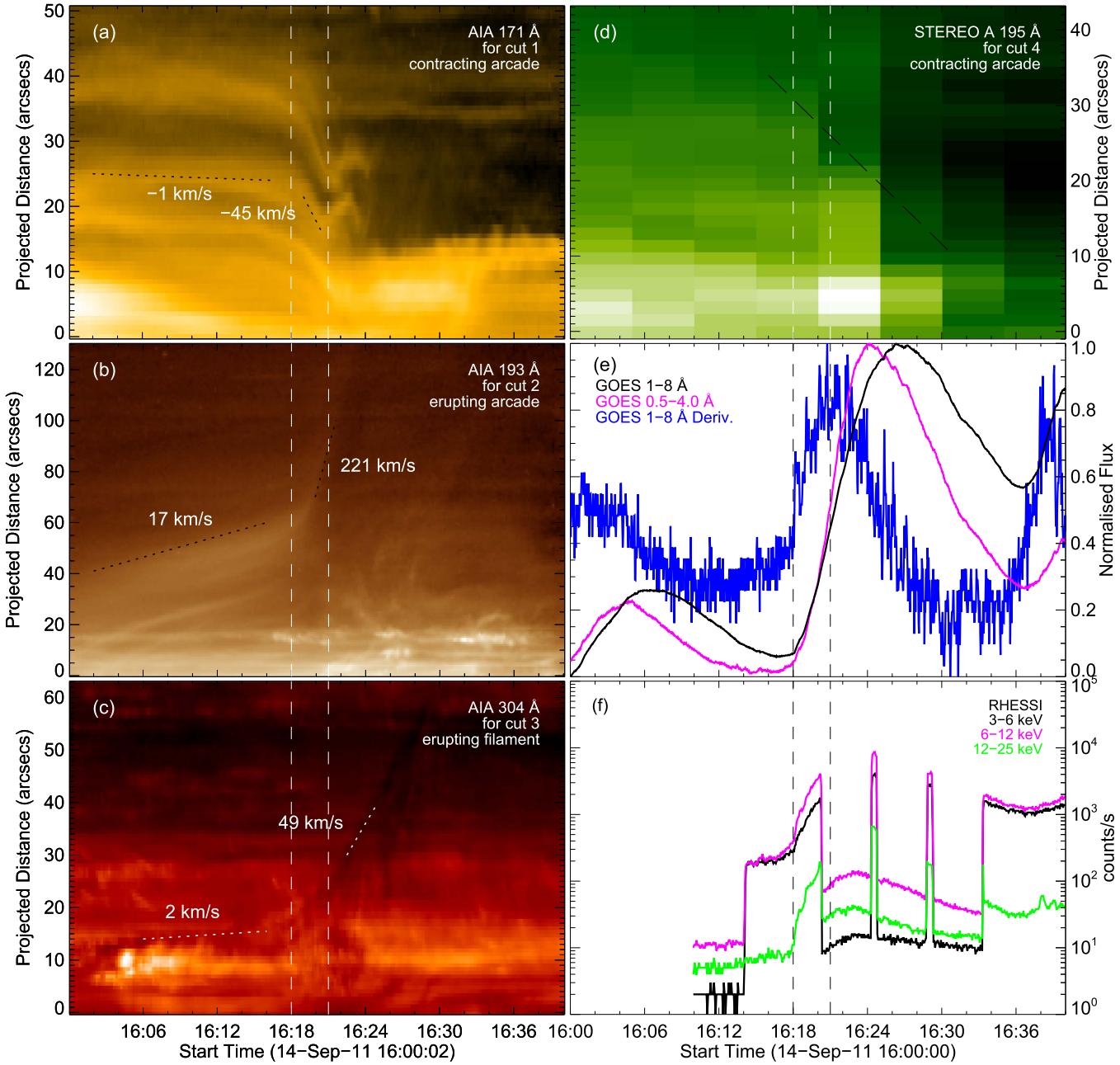

Figure 2. (a)–(d) Timeslices for dynamic features in Event I. The sampling time of *STEREO A* 195 Å in (d) starts from the beginning of each timeslice, with an exposure duration ∼8 s, and the long-dashed line shows the rough contraction trend but means an uncertain contraction speed because of the long sampling cadence ∼5 minutes and few sampling points. (e)–(f) *GOES* and *RHESSI* light curves, respectively. The two vertical dashed lines across the figure show the time interval of the arcade contraction.

2. Observations and Analyses

We select four events, SOL2011-09-14T16:26 (C4.2), SOL2014-02-17T23:15 (C1.9), SOL2016-04-08T01:56 (B8.3), and SOL2016-11-22T23:45 (B6.0), for analysis, which are located in active regions NOAA 11290 (S17W47), 11978 (N05W89), 12529 (N09E88), and 12612 (N11E89). Hereafter, for convenience, the four events are labeled as Events I, II, III, and IV, respectively. They are all observed by both the *Solar Dynamics Observatory*/Atmospheric Imaging Assembly (*SDO*/AIA) and *STEREO A*. The contracting arcades in these four events all have an almost edge-on geometry from the perspective of AIA, so the contributions to the loop dynamics from contraction and inclination can be clearly disentangled. The contracting loops observed by *STEREO A* in 195 Å are very likely the same as that viewed from AIA in 193 Å (for Event IV the contracting structures in 171 Å are similar to that in 193 Å), because (1) these two wave bands share similar observing temperature $\sim 1.5 \times 10^6$ K; (2) the structures observed from the two perspectives show expected positions and geometry according to the relative positions of *SDO* and *STEREO*; and (3) there are good temporal correspondences between the contracting motions captured by the two observatories. AIA images and photospheric magnetograms from Helioseismic and Magnetic Imager (HMI) for Event I have been processed by the standard software (Boerner et al. 2012), and supplementary images from *STEREO A* via secchi_prep.pro (Howard et al. 2008).

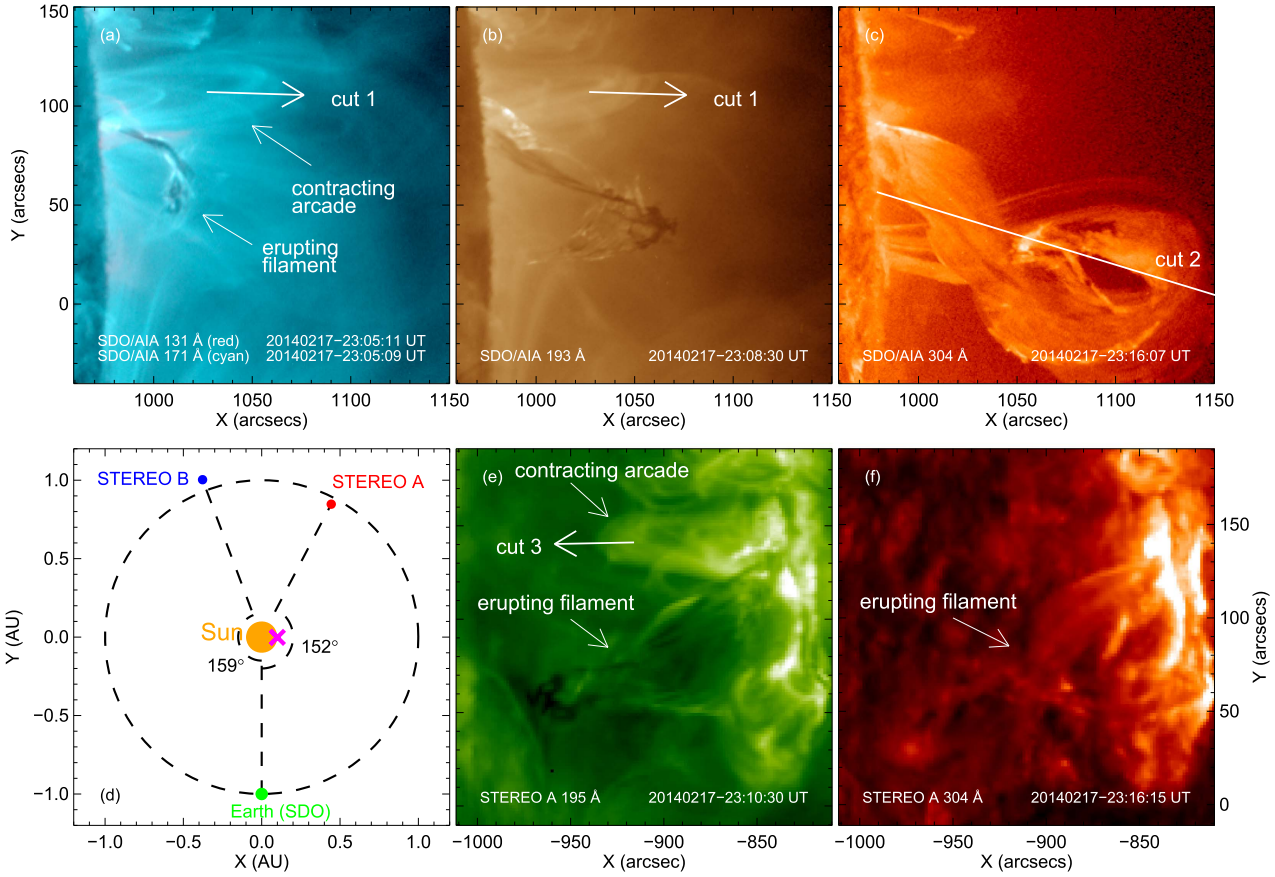

Figure 3. Images for Event II SOL2014-02-17T23:15. (a)–(c) Observed from the perspective of AIA; 131 Å is red, and 171 Å is cyan in (a). (d) Relative positions of *SDO* and *STEREO*. The magenta cross shows the longitudinal position of the event. (e)–(f) Observed from the perspective of *STEREO A*. Cuts 1–3 are used for the timeslices in Figure 4. The arrowhead of cut 2 is beyond the image edge. The animation compares panels (a), (b), (e), and (f) for Event II from 2014 February 17 22:50 to 2014 February 18 00:20 UT.

(An animation of this figure is available.)

2.1. Event I: SOL2011-09-14T16:26

Event I is shown in Figure 1 and the accompanying animation, with both AIA and *STEREO A* observations. AIA observes the contracting arcade (hereafter, we call it arcade I) from the side with a nearly horizontal geometry (Figures 1(a) and (b)), while *STEREO A* looks at it from the top with the loop plane having ∼45° with respect to the line of sight (Figure 1(e)). A filament is located low in the corona (Figure 1(c)). As it is destabilized and erupts outward (Figure 1(f)), another arcade structure (hereafter, arcade II) passes from beneath arcade I and erupts (Figure 1(b)). Meanwhile, arcade I contracts toward the space left by the erupting filament and arcade II. The motion of contraction is unambiguous, which is evidenced by the accompanied animation. Oscillation follows and finally most of the loops of arcade I disappear.

Figure 2(a)–(d) show the timeslices created along the cuts 1–4 chosen in Figure 1, respectively, presenting the detailed dynamics of the corresponding features along the cuts. The major contraction of arcade I (in the interval between the two dashed lines) starts as the filament and arcade II erupt, though they already have similar but weaker behaviors before this time interval. This major contraction interval also corresponds to the rise of the impulsive phase, which is illustrated by the *GOES* 1–8 Å derivative in Figure 2(e) and the light curve of *RHESSI* 12–25 keV in Figure 2(f). After the major contraction, the loops of arcade I oscillate and most of them disappear (Figure 2(a)), though the filament and arcade II still continue to move outward rapidly (Figures 2(b) and (c)). We note that the contraction speed of arcade I is always much smaller than the eruption speeds of arcade II and also the filament. The filament eruption speed is underestimated in Figure 2 because of projection, and can be more accurately estimated to be ∼150 km s^{-1}, by considering the time interval between 16:18:00 UT (the start time of the filament eruption from Figure 2(c)) and 16:26:15 UT (Figure 1(f)), and the travel distance ∼100 arcsecs in Figure 1(f). The final contraction distance of arcade I is also much smaller than the final eruption distances of the filament and arcade II.

2.2. Event II: SOL2014-02-17T23:15

Figures 3 and 4 are constructed similarly to Figures 1 and 2, respectively. Event II is located on the limb with a more favorable perspective, making the contraction of the arcade clearer. Seen from the accompanying animation, first the filament lies close to the solar surface, with the arcade overlying its northern end. Then they expand upward simultaneously up to around 23:05 UT (Figure 3(a)). As the filament starts to writhe along with its southwestward eruption (Figure 3(b)), the arcade begins to contract and the northern end of the filament seems to be pushed downward to the solar

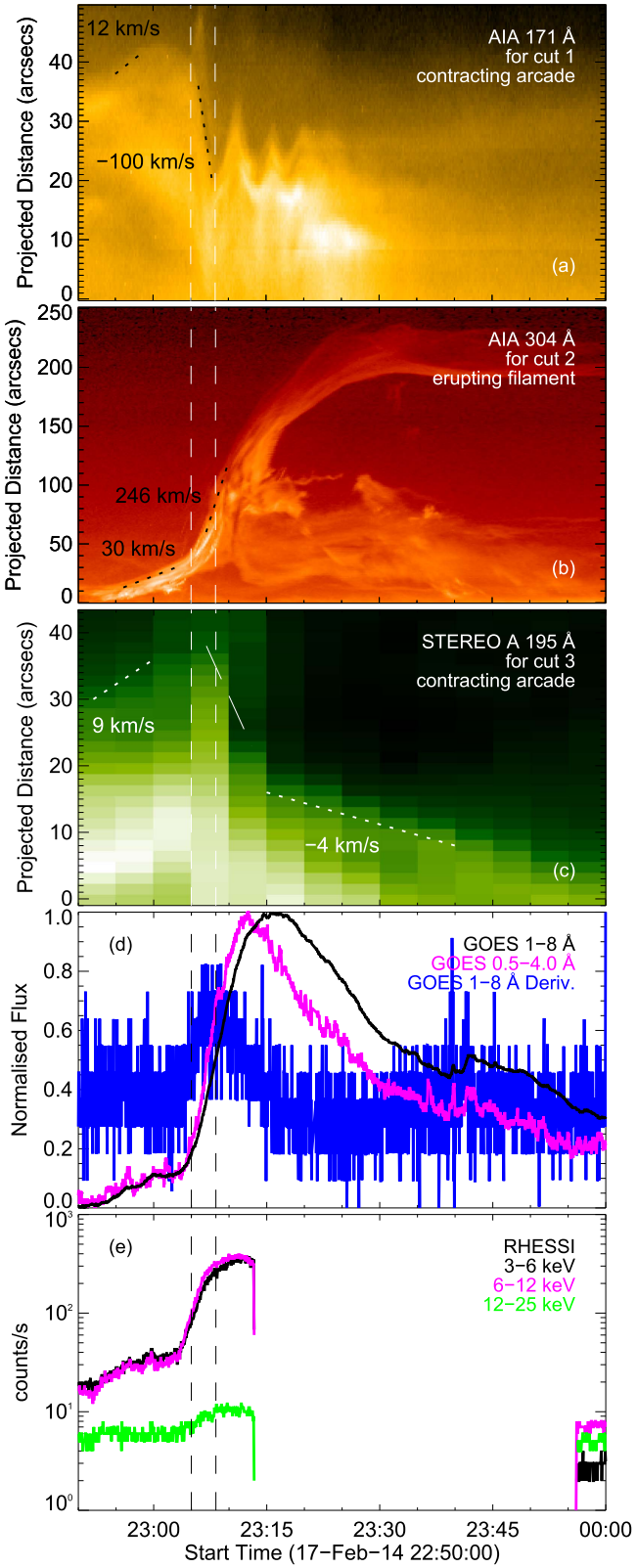

Figure 4. (a)–(c) Timeslices for dynamic features in Event II. The sampling time of *STEREO A* 195 Å in (c) starts from the beginning of each timeslice, with an exposure duration ∼8 s, and the long-dashed line shows the rough contraction trend but means an uncertain contraction speed because of the long sampling cadence ∼5 minutes and few sampling points. (d)–(e) *GOES* and *RHESSI* light curves, respectively. The two vertical dashed lines across the figure show the time interval of the arcade contraction.

surface. In the end, the arcade oscillates and gradually disappears.

Similar to Event I, the major arcade contraction coincides with the beginning of the filament eruption and the rise stage of the impulsive phase, and the arcade contracts more slowly and over a much smaller distance than the filament erupts (Figure 4). Event II differs from Event I in that before the major contraction, the arcade in Event II shows slow expansion rather than slow contraction as in Event I.

2.3. Event III: SOL2016-04-08T01:56

AIA and *STEREO A* observe the contracting arcade in Event III from opposite sides (Figures 5(a), (b), and (e)). The arcade contracts as a flare underneath happens (Figure 5(b)). Strangely, neither AIA nor *STEREO* observations, which together have a wide temperature coverage (including cool 304 Å, warm 171, 193, and 195 Å, and hot 131 Å), show any signatures of violent arcade or filament eruptions such as those seen in Events I and II. There is only another arcade in the south expanding outward to a small extent (Figure 5(b)). The arcade in the north fades into the flaring region at the end with no obvious oscillation detected.

Figure 6(a) shows that the speed of the long-duration arcade contraction is only a few km s^{-1}, which is slow but real, rather than caused by solar rotation, because there are surrounding static loops as a reference (see the accompanying animation). Interestingly, an abrupt acceleration in the contraction occurs at around 01:20 UT, which coincides with a sudden increase or a spike in the *GOES* 1–8 Å light curve (Figure 6(d)). It seems that the contraction of the arcade is quite sensitive to the flare. Though the Neupert effect is not notable here, the contraction process has already continued past the peak of the *GOES* 1–8 Å flux, which means that the arcade contraction spans the entire impulsive phase. This is unlike the situations in Events I and II, where the contraction is localized in time to the rise of the impulsive phase. The expansion speed of the arcade in the south is also very small (Figure 6(b)), comparable to the contraction speed of the arcade in the north, but it only persists for about half of the contraction interval, which results in an expansion distance of around half of the contraction distance.

2.4. Event IV: SOL2016-11-22T23:45

In Event IV, AIA observes two contracting arcade systems with an edge-on geometry (see Figure 7(a) and accompanied animation). Unlike the situation in Zuccarello et al. (2017), where the two peripheral arcades first diverge from each other and then contract, these arcades here directly converge toward each other and contract at the same time (Figure 7(b)). As they do so, it seems that two flare regions from two sides approach to the convergence location, which may imply that magnetic energy is released gradually toward the central core region. From *STEREO A*, we also detect the arcade contraction, with a face-on geometry (Figure 7(e)). The final disappearance of the contracting arcades is also found here without notable oscillation. Similar to Event III, there are no violent arcade or filament eruptions observed by the two instruments, but only a minor arcade expansion in AIA (Figure 7(b)). From the animation, it appears that this small expansion might be associated with a very weak invisible flux rope erupting

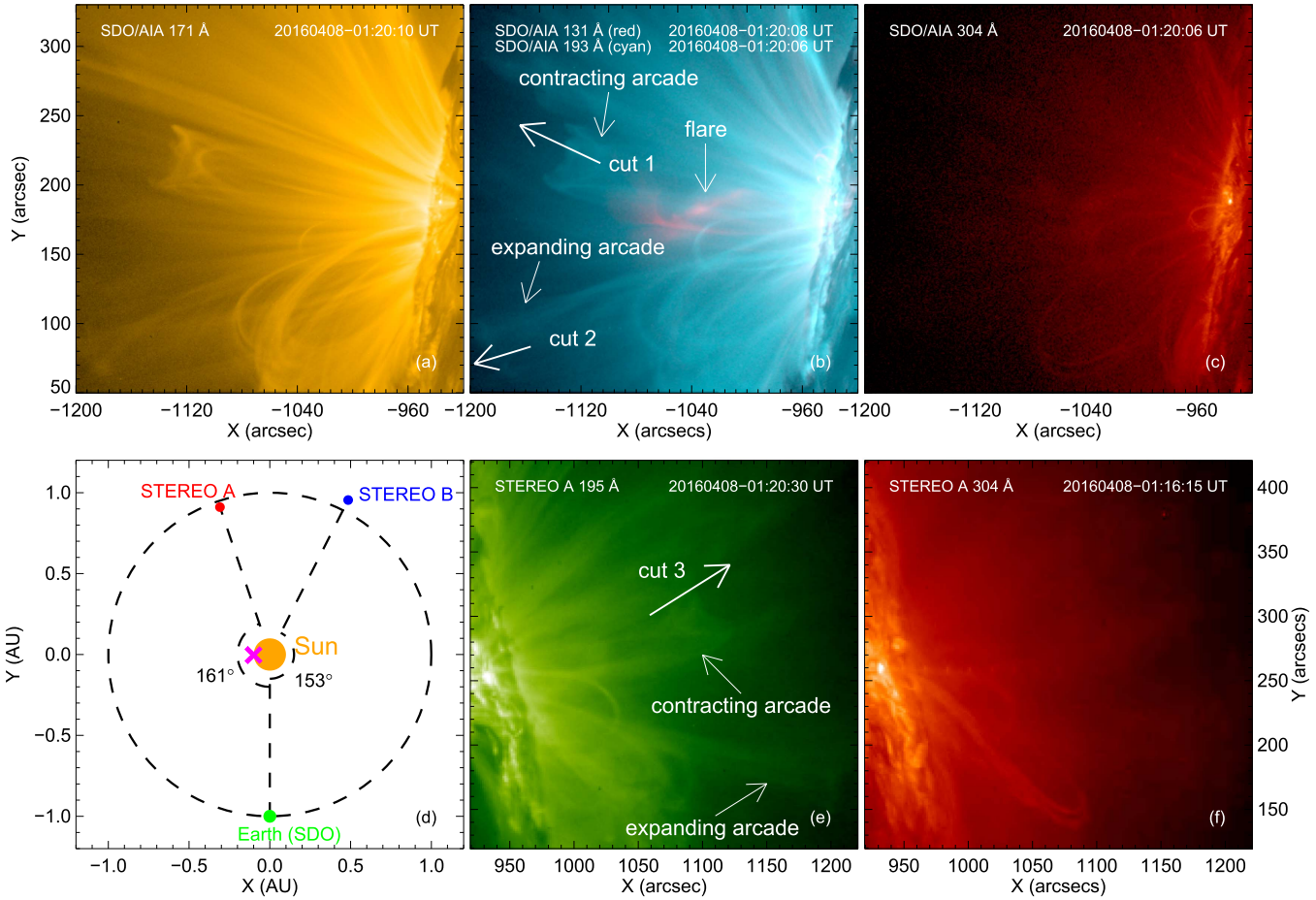

Figure 5. Images for Event III SOL2016-04-08T01:56 B8.3. (a)–(c) Observed from the perspective of AIA; 131 Å is red, and 193 Å is cyan in (b). (d) Relative positions of *SDO* and *STEREO*. The magenta cross shows the longitudinal position of the event. (e)–(f) Observed from the perspective of *STEREO A*. Cuts 1–3 are used for the timeslices in Figure 6. The animation compares panels (a), (b), (e), and (f) for Event III from 2016 April 07 23:50 to 2016 April 08 02:30 UT.

(An animation of this figure is available.)

outward, or it could also be a field line opening due to magnetic reconnection.

Different from Events I and II, the arcade contraction speed in this event is much larger than the expansion speed (Figures 8(a) and (b)). More similarities are found between Events III and IV. The contraction distance is much larger than the expansion distance, and it also happens during the entire impulsive phase (Figures 8(d) and (e)).

3. Discussion

3.1. Observational Characteristics

Unlike previous observations of contracting loops on the solar disk, which are plagued by projection effects, we believe that the main contributing factor for the motion of the loops observed from the perspective of *SDO*/AIA for the four events presented here is real contraction of loops seen approximately edge-on, and the argument for this is as follows. (1) It seems unlikely that they could actually be tall and narrow loops seen face-on, otherwise the pointed cusp would drag the loop to contract under magnetic tension force even before the event happens, which is not the case in observations. (2) Due to the edge-on property, we can easily exclude the possibility that the shrinking is due to significant loop inclining perpendicular to its plane, though minor changes in inclination can be observed (especially in Events I and II). (3) As large-scale peripheral loops usually have a dipole geometry, they would not be expected to bend or distort in their own plane so we can exclude apparent shrinkage due to this (even though in some cases they might happen under the impact of nearby erupting structures, they would restore to their original positions after the eruption completes, which is not observed here; and it is rare to see dramatic loop inclining in its plane when viewed on the solar disk with a face-on geometry; even in Events III and IV, there are no violent eruptions). (4) The last option left to explain the apparent contraction seems to be a real and significant contraction of the loops.

Table 1 summarizes the relevant information about the four selected events on the large scale. We concentrate on their eruptiveness, dynamic timing, distance, and speed, which can separately reflect the onset, duration, total amount, and rate of associated energy change. Both Events I and II exhibit violent filament (or arcade) eruptions in close proximity to the contracting arcades (Figures 1(b) and 3(a)), whereas there are only small expansions of arcades (or at most signatures of very weak, invisible flux rope eruptions) during the arcade contractions for Event III and IV (Figures 5(b) and 7(b)). The arcades in Events I and II mainly contract at the rise stage of the impulsive phase. By contrast, the arcade contractions respond to their entire impulsive phases in Events III and IV.

In terms of dynamic timing, distance, and speed, Events I and II show the typical characteristics of eruptive flares, with

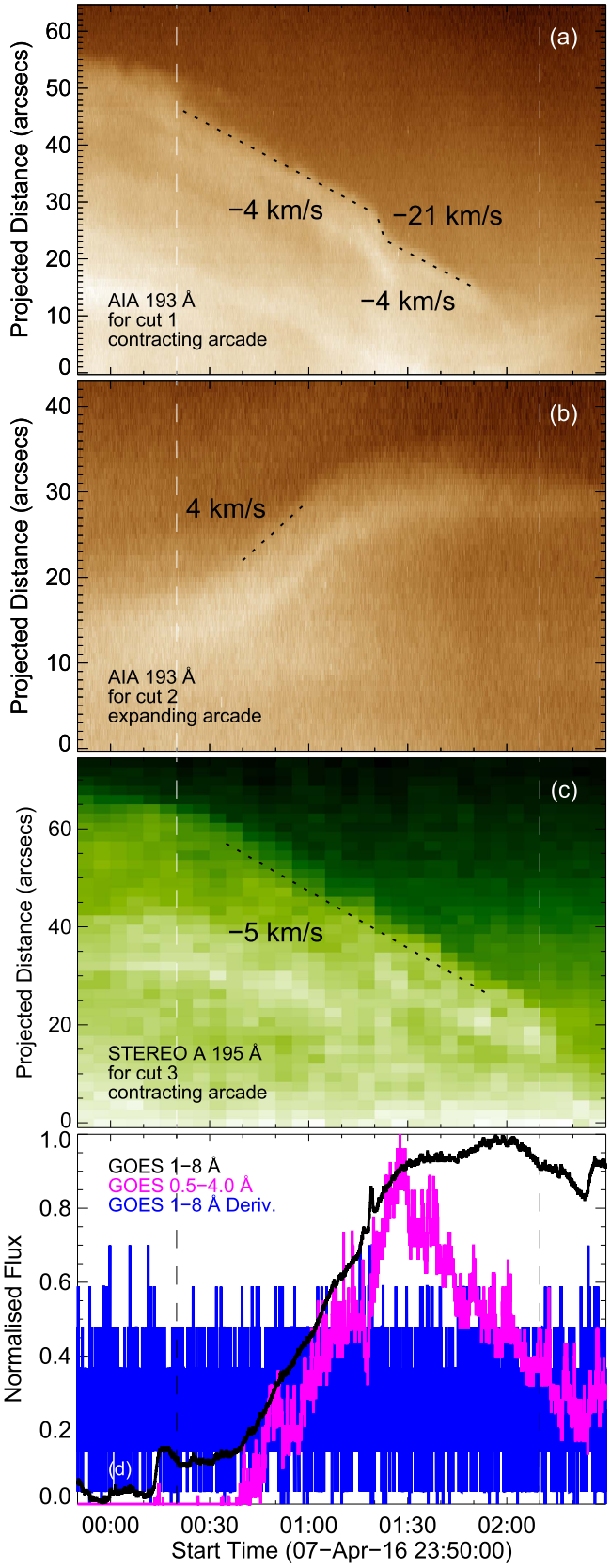

Figure 6. (a)–(c) Timeslices for dynamic features in Event III. The sampling time of *STEREO A* 195 Å in (c) starts from the beginning of each timeslice, with an exposure duration ∼8 s. (d) *GOES* light curves. The two vertical dashed lines across the figure show the time interval of the arcade contraction.

eruption processes prominent in the large-scale dynamics; though, the vast majority of eruptive flares are not accompanied by observed arcade contractions like those reported here. Events III and IV seem to have the opposite trend as the arcade contraction process dominates over the expansion/eruption on the large scale. This new type of coronal evolution may present a great challenge to eruptive flare models, like the "CSHKP" standard model (Carmichael 1964; Sturrock 1966; Hirayama 1974; Kopp & Pneuman 1976) or breakout model (Antiochos et al. 1999; Aulanier et al. 2000).

3.2. Underlying Physics

What is the physics behind these arcade contraction phenomena? And what causes them to show the two different categories above in Table 1? The implosion conjecture proposed by Hudson (2000) provides a possible explanation. In his original paper, it was realized that both eruptions and flares as two main approaches to release magnetic energy stored in the corona could cause implosions. As eruptions and flares may involve different evolutionary timescales and large-scale dynamics, naturally, we would expect to detect two kinds of implosion processes separately associated with them, characterized by different properties. This analysis raises a likely interpretation of the two kinds of arcade contraction behaviors observed, i.e., eruption-driven implosions and flare-driven implosions.

The distinctions between these events in Table 1 seem to match this expectation. Violent filament (or arcade) eruptions are seen in Events I and II, dynamically related with the arcade contractions, which may indicate that they are eruption-driven implosions. On the contrary, with no such noticeable large-scale eruptions and only flares detected, Events III and IV may represent flare-driven implosions. Supporting evidence comes from the time range during which the contraction happens. In Events III and IV, the arcades contract during the entire impulsive phase, which is expected from the flare-driven scenario, because the flares continually release coronal magnetic energy and reduce the corresponding pressure. However, in Events I and II, the major contractions only occur before the peak (or during the rise stage) of the impulsive phase, even though the flares still continue to liberate significant energy in the rest of the impulsive phase. This thus reflects a different responsible source. This could be the associated filament (or arcade) eruptions, as the escape time from the innermost core regions could be shorter than the flare duration. Since in a few well-observed events (Sun et al. 2012; Simões et al. 2013; Wang et al. 2016, and Events I and II here) we notice that the inner loops, closer to the core region, stop contracting almost at the peak of the impulsive phase, we suggest that it is around this time that the filament escapes from the innermost core region. In the spirit of this argument, the much slower contraction after the major contraction of Event II (Figure 4(c)) might be interpreted as caused by the ongoing flare just underneath the contracting arcade (see Figure 3 and accompanying animation). The dominance in distance and speed of the eruptions in Events I and II is in accordance with the expectation of the arcade contractions being merely an auxiliary in the global dynamics, whereas the contractions play a more prominent role on the large scale than the expansions/eruptions in Events III and IV, supporting a different triggering source, which could be the flares. In particular, the coincidence

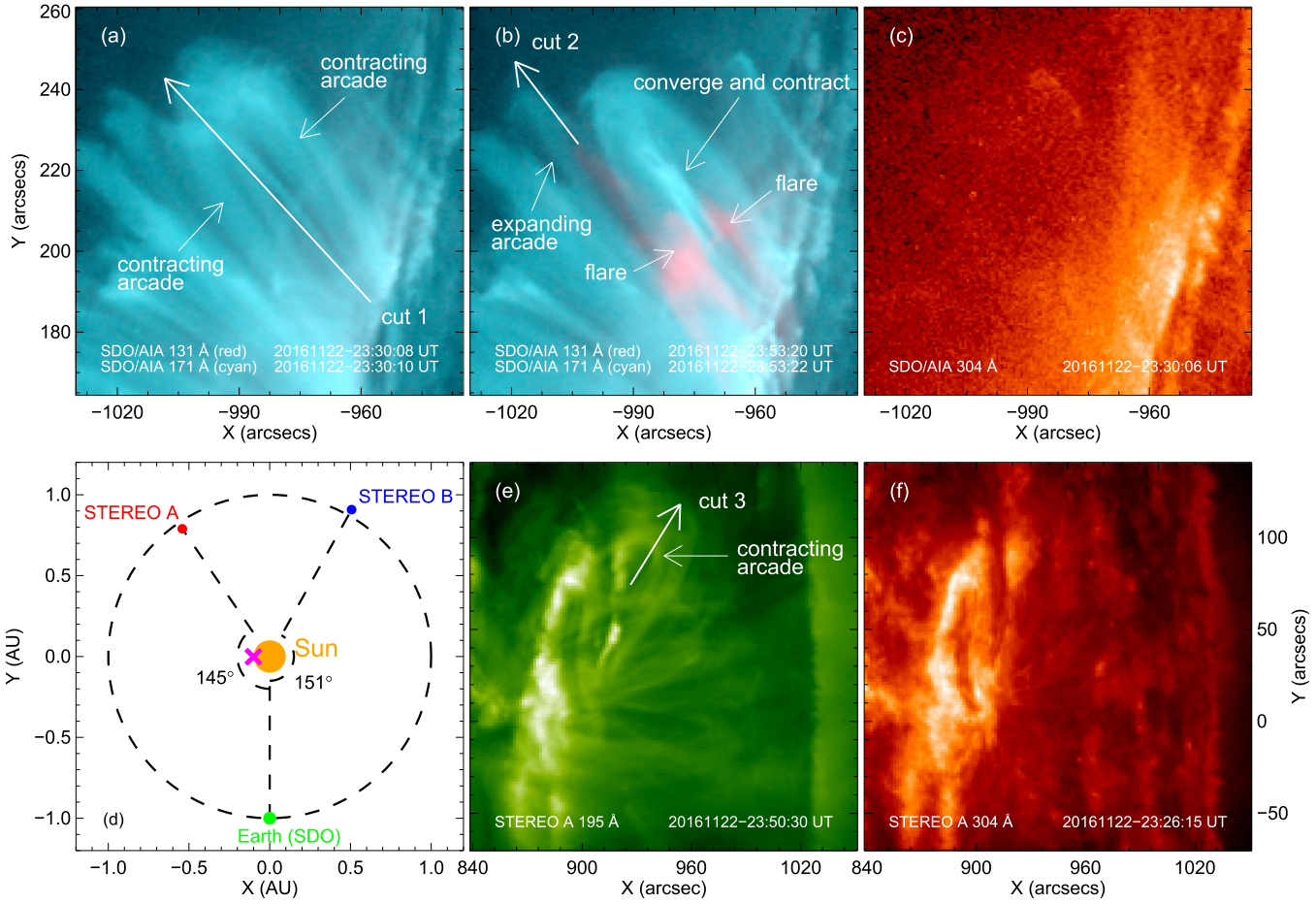

Figure 7. Images for Event IV SOL2016-11-22T23:45 B6.0. (a)–(c) Observed from the perspective of AIA. 131 Å is red, and 171 Å is cyan in (a) and (b). (d) Relative positions of *SDO* and *STEREO*. The magenta cross shows the longitudinal position of the event. (e)–(f) Observed from the perspective of *STEREO A*. Cuts 1–3 are used for the timeslices in Figure 8. The animation compares panels (a), (b), (e), and (f) for Event IV from 2016 November 22 23:30 to 2016 November 23 01:00 UT. (An animation of this figure is available.)

of the abrupt acceleration of the contraction and the spike in *GOES* 1–8 Å flux at ∼01:20 UT in Event III (Figure 6) implies a close connection between these two phenomena.

3.3. Models

Figure 9 illustrates our understanding of these four events exploiting the implosion conjecture. Figures 9(a)–(b) and Figures 9(c)–(d) describe the field evolution of Events I and II, respectively. As argued above, Events I and II are of eruption-type, and thus possess similar essential dynamic characteristics, i.e., when the underlying filament erupts outward, the peripheral overlying arcade contracts. This scenario is also used to interpret the event in Wang et al. (2016). The basic idea is that filament (or arcade) field redistribution, and/or conversion of its energy to kinetic and gravitational energy, can locally reduce magnetic energy and pressure in its original position, resulting in forces in the periphery being unbalanced and the associated loops contracting. Another interesting explanation by Zuccarello et al. (2017) and Dudík et al. (2017) is that the eruption and contraction in this MHD situation are an analog of a fast flow creating vortices in its surroundings in hydrodynamics. However, due to the preferable perspectives here, we see that, in Event I (see Figure 1 and the accompanying animation) arcade I just adjacent to arcade II contracts directly when arcade II erupts, without the significant initial expansion and inclination phases that are expected in the vortex-flow scenario (Dudík et al. 2017). And in Event II the arcade only shows an arc-like flow rather than a complete vortex trajectory in the hydrodynamic situation, which is also illustrated in Figure 9(d). In theory, the viscous term in the invoked momentum equation (Aulanier et al. 2005; Zuccarello et al. 2015) of the simulation performed by Zuccarello et al. (2017) and Dudík et al. (2017) is much smaller than the Lorentz force in a low β coronal MHD environment. Thus, the viscosity, which is responsible for vortex generation in the hydrodynamic case, would not be able to create the large-scale organized rapid contraction behaviors, though it might produce small-scale vortices around the erupting structure. The large-scale dynamics is controlled by the dominant Lorentz force. Zuccarello et al. (2017) argued that it is the enhanced magnetic tension, one component of the Lorentz force, caused by compressional Alfvén waves originating from the erupting field, that generates the contraction flow, but according to this argument, the contracting loops are expected to restore to their original locations after the filament (or arcade) erupts completely because of the nature of waves, which does not agree with the reported observations in which the loops remain at lower altitudes. Similarly, if the contracting motion was only caused by enhanced magnetic pressure (the other component of the Lorentz force) above the loops due to the erupting structure,

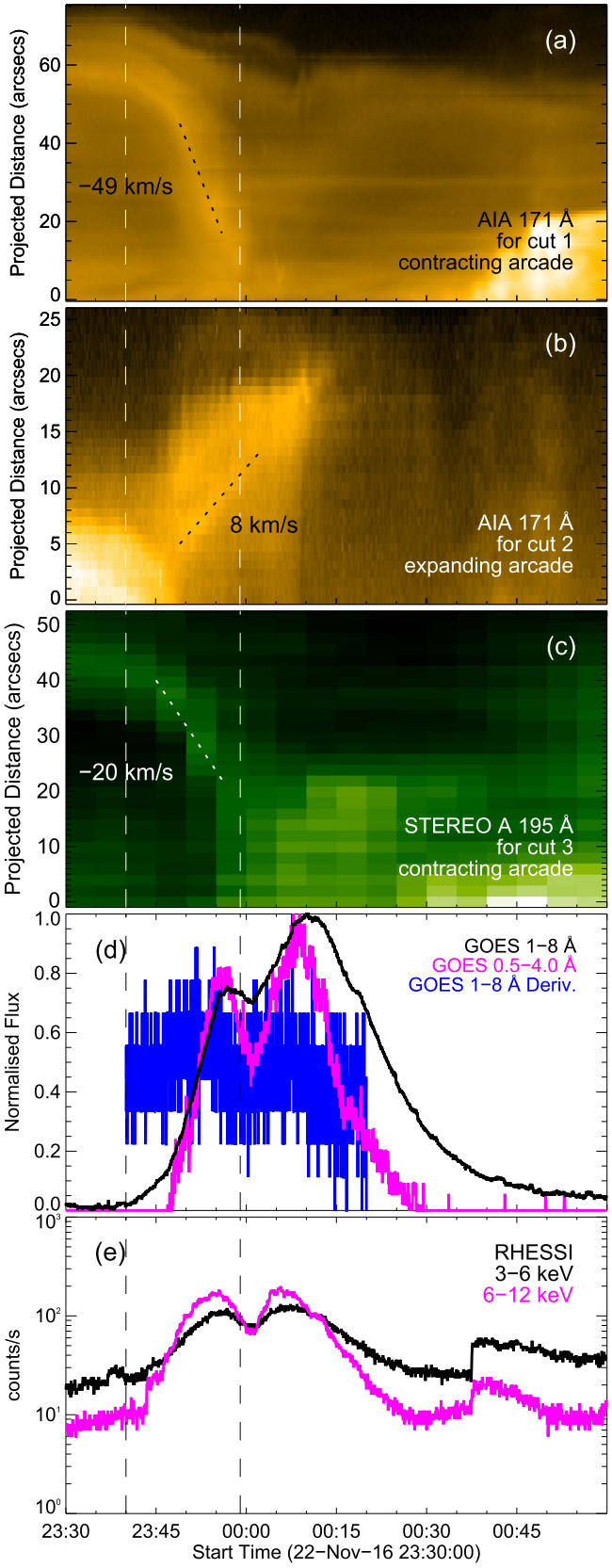

Figure 8. (a)–(c) Timeslices for dynamic features in Event IV. The sampling time of *STEREO A* 195 Å in (c) starts from the beginning of each timeslice, with an exposure duration ∼8 s. (d)–(e) *GOES* and *RHESSI* light curves, respectively. The two vertical dashed lines across the figure show the time interval of the arcade contraction.

we would also expect their restoration when the eruption terminates, not conforming to the observations either.

The final idea then resorts to reduced magnetic pressure underneath, which is just the core idea of the implosion conjecture. In fact, the arc-like flow in Figure 9(d) can be easily explained in this framework. As the filament erupts outward, the magnetic pressure is enhanced at higher altitude and reduced at lower altitude, which would naturally induce an arc-like flow of a peripheral unopened arcade field around the central erupting structure because of pressure difference compared to the previous equilibrium state. Depending on the detailed topology and eruption process, the arc-like flow may not be so obvious in some cases, like Event I here; and the loops located at lower altitudes where they are not severely impacted by the high-pressure erupting structure could also contract directly, e.g., the event in Simões et al. (2013). The perturbation in the pressure should propagate outward with a limited speed, as observed by Simões et al. (2013) in a face-on geometry. This could be the fast-mode speed (∼Alfv́en speed v_A if plasma $\beta \ll 1$ as in the corona).

Particularly, there is strong observational evidence that Events III and IV do not show violent eruptions and vortex-like or even arc-like flows. The arcade in Event III contracts directly, and the two arcades of Event IV even converge toward each other and simultaneously contract downward. The contractions are significantly different from peripheral vortices created by a central fast flow in hydrodynamics, and thus cannot be explained by the analogy. Instead, the implosion conjecture (Hudson 2000) is able to account for these two events, in terms of flare-driven implosions, without the need for eruptions. This has already been supported by the distinct properties of Events III and IV in Table 1, as argued above. Because of a mix of difficulties from limb location, structure overlapping in an edge-on geometry, and low contrast, the 3D field topologies of Events III and IV are not readily reconstructed. However, we propose a general model for them to interpret the major contractions and minor expansions observed, based on the implosion conjecture. Figures 9(e)–(f) illustrate the basic idea. The "black box" underlying the two arcade systems represents the core region where a flare occurs. During the flare, the total magnetic energy and pressure are reduced within the entire "black box." However, there could exist a situation where the field energy underneath arcade III decreases and that underneath arcade IV increases, but the increase under arcade IV is smaller than the decrease under arcade III. Then we would expect to see that the contraction of arcade III is larger in extent and faster in speed than the expansion of arcade IV, which would then be in agreement with the properties of Events III and IV in Table 1. However, the detailed field reconnection process, corresponding topology change and energy transport and dissipation in the "black box" are unclear. The magnetic energy enhancement underneath arcade IV might be due to more closed field formed or field opening there through reconnection between the two domains under the two arcade systems. Such a model of flare-driven implosions is attractive and can reproduce the observations in a general way, but another possibility, which cannot be completely excluded, is that a small and invisible flux tube may continuously transport from under arcade III toward arcade IV, in the spirit of eruption-type implosions but a very weak one.

Table 1
Focused Large-scale Properties of the Four Selected Events

	SOL2011-09-14T16:26 Event I	SOL2014-02-17T23:15 Event II	SOL2016-04-08T01:56 Event III	SOL2016-11-22T23:45 Event IV
Eruptiveness	possess visible, significant filament (or arcade) eruptions		only have small and weak arcade expansions; no obvious filament (or arcade) eruptions	
Timing	mainly contract during the rise stage of the impulsive phase		contract during the entire impulsive phase	
Distance	arcade contraction distance (Event I: $\sim$10 arcsec; Event II: $\sim$20 arcsec) is much smaller than filament (or arcade) eruption distance (Event I: $>$ 70 arcsec; Event II: $\sim$200 arcsec)		arcade contraction distance (Event III: $\sim$40 arcsec; Event IV: $\sim$45 arcsec) is much larger than arcade expansion distance (Event III: $\sim$15 arcsec; Event IV: $\sim$15 arcsec)	
Speed	arcade contraction speed (Event I: $\sim$45 km s^{-1}; Event II: $\sim$100 km s^{-1}) is much smaller than filament (or arcade) eruption speed (Event I: $\sim$221 km s^{-1}; Event II: $\sim$246 km s^{-1})		arcade contraction speed (Event III: $\sim$5 km s^{-1}; Event IV: $\sim$49 km s^{-1}) is comparable to, or much larger than arcade expansion speed (Event III: $\sim$4 km s^{-1}; Event IV: $\sim$8 km s^{-1})	
Possible Origin	eruption-driven implosions		flare-driven implosions	

Note. For Events III and IV, the expanding structures could incline toward or away from *SDO*, resulting in underestimations of their traveling distances and speeds, but from the accompanied animations and geometry, it seems that they do not incline too much. If we assume the inclination angle to be a characteristic value $\sim$45°, the conclusions here still hold, not to mention that the contracting structures could not be in the sky plane as well.

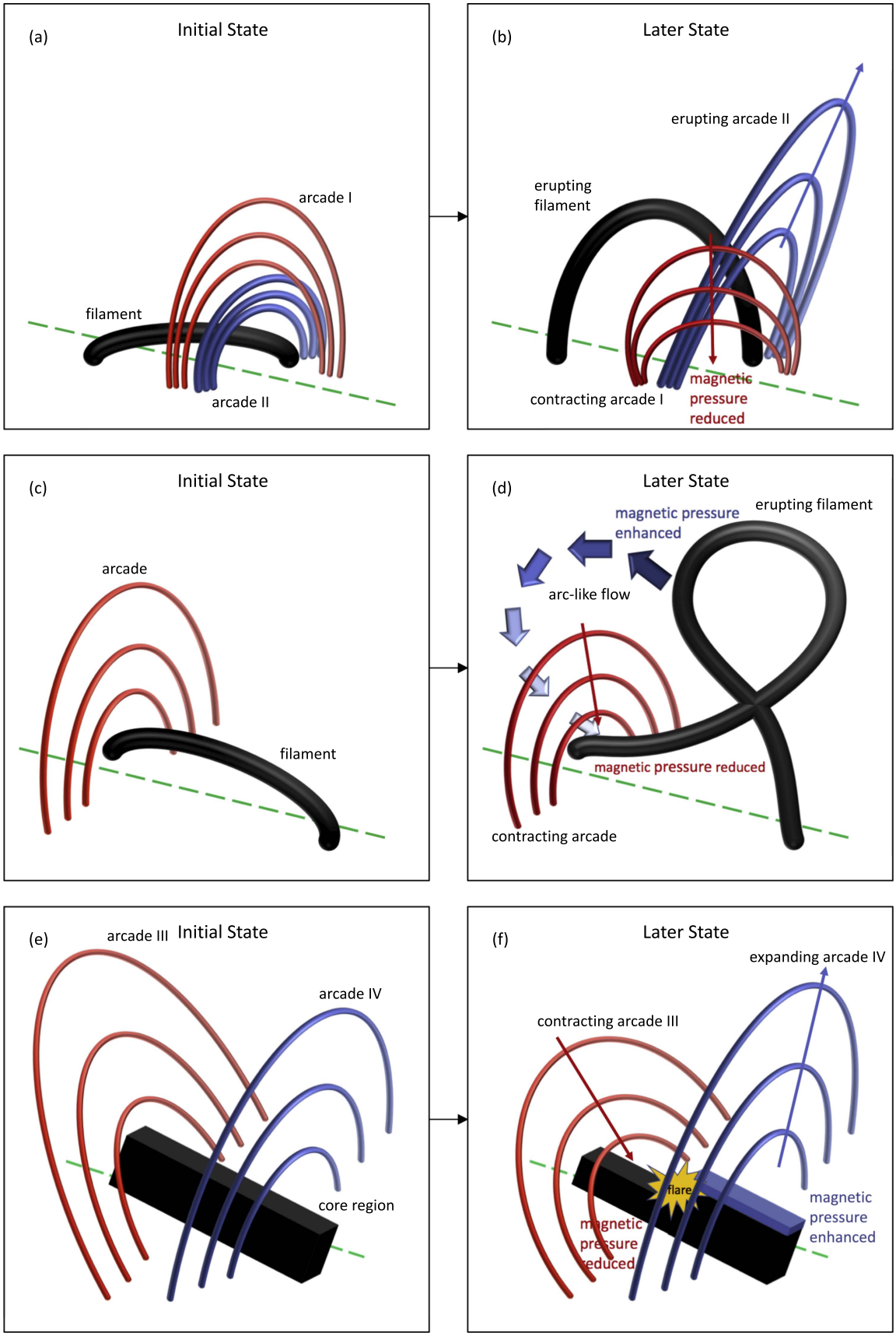

Figure 9. Cartoons show our understanding of the implosion events. (a)–(b) For Event I. (c)–(d) For Event II. (e)–(f) For Events III and IV. The thin arrows in each image indicate the directions of the implosion and expansion motions of the arcades. And the green dashed line represents the polarity inversion line.

3.4. Unsuccessful Implosion

It is worth noting that well-observed implosions, either face-on or edge-on remain rather rare, whereas the implosion conjecture implies that they should be present in all solar energy-releasing events, including eruptions and flares. This is probably because of unfavorable viewing, complexity of the active region field and reconnection processes involved (Liu & Wang 2010), or relatively small expected movements in readily observed peripheral loops when a relatively small fraction of active region energy is released in the core region in a flare. However, in this context, we would like to revisit one of the original assumptions for the implosion conjecture in Hudson (2000), i.e., that gravity plays no significant role in the coronal dynamics. This might not always be the case, especially when a filament is involved, and this could lead to unsuccessful implosions. Take the illustrations Figures 9(c)–(d), for example, in a general way (rather than considering the specific Event II). Suppose, as a thought experiment, that before the eruption in Figure 9(c), the filament is mass loaded, with the downward gravitational force contributing a non-negligible amount to the force balance against the upward Lorentz force. Now imagine what would happen if, simultaneously with the MHD instability, much of the material along the filament drained down to the photosphere. As the local plasma density and thus gravitational pull are reduced, the filament field would inflate, simultaneously pushing the overlying arcade outward, which is the opposite of an implosion. Similarly, during the eruption in Figure 9(d), such a process would occur if mass along the filament field could drain down (see relevant studies, e.g., Fong et al. 2002; Bi et al. 2014; Fan 2017; Jenkins et al. 2018, pointing out that substantial filament material drains down that may influence the dynamics) and also spread into a larger volume. Moreover, as the filament field becomes more vertical, the draining could increase, further inflating the surrounding field. Thus the overlying arcade would expand if the magnetic energy change associated with the filament is not considered. However, in fact, the filament field becomes "weaker" locally, distributing into a larger volume and transferring its energy into plasma kinetic and gravitational energy. As argued by Hudson (2000) and Russell et al. (2015), to achieve a new equilibrium, the overlying arcade would implode toward the magnetic-pressure-reduced filament. At the end, in this scenario, we would have two competing mechanisms controlling the dynamics: gravity reduction making the field expand and magnetic pressure reduction making the field implode. In some cases, the magnetic pressure reduction is dominant so we see implosions, like Events I and II here, while the gravity reduction may overtake in other situations, which might be one of the reasons for rarity of well-observed implosions.

4. Conclusions

With the four selected events having the up-to-now most clearly observed continuously contracting loops in an edge-on geometry from the viewpoint of *SDO*/AIA, supplemented by observations from *STEREO*, for the first time, we demonstrate the existence of real contractions of loops in the global coronal dynamics unambiguously. The implosion conjecture proposed by Hudson (2000) in the interpretation of these events is found to be effective, in comparison with alternative theories for which disagreements currently exist between observations and simulations or other predictions. Meanwhile, the discussion also leads us to find two implosion categories that can be associated either with solar eruptions or with flares, and the models put forward according to the conjecture can reasonably explain their distinct observational characteristics. However, it is also pointed out that in some cases the implosion scenario may not be valid as one of the original assumptions about the role of gravitation in the dynamics may fail.

The authors thank the referee for very helpful comments and suggestions, which significantly improve the quality of the manuscript, and Hugh Hudson for a discussion. L.F. and P.J.A.S. acknowledge support from STFC Consolidated Grant ST/L000741/1 and ST/P000533/1. P.J.A.S. acknowledges support from the University of Glasgow's Lord Kelvin Adam Smith Leadership Fellowship. The authors are grateful to NASA/*SDO*, AIA, HMI, *STEREO*/EUVI, and *GOES* science teams for data access.

Facilities: *SDO*(AIA and HMI), *STEREO*(EUVI), *GOES*.

ORCID iDs

Juntao Wang https://orcid.org/0000-0001-9268-2966
P. J. A. Simões https://orcid.org/0000-0002-4819-1884
L. Fletcher https://orcid.org/0000-0001-9315-7899

References

Antiochos, S. K., DeVore, C. R., & Klimchuk, J. A. 1999, ApJ, 510, 485
Aulanier, G., DeLuca, E. E., Antiochos, S. K., McMullen, R. A., & Golub, L. 2000, ApJ, 540, 1126
Aulanier, G., Démoulin, P., & Grappin, R. 2005, A&A, 430, 1067
Bi, Y., Jiang, Y., Yang, J., et al. 2014, ApJ, 790, 100
Boerner, P., Edwards, C., Lemen, J., et al. 2012, SoPh, 275, 41
Carmichael, H. 1964, NASSP, 50, 451
Dudík, J., Zuccarello, F. P., Aulanier, G., Schmieder, B., & Démoulin, P. 2017, ApJ, 844, 54
Fan, Y. 2017, ApJ, 844, 26
Fan, Y., & Gibson, S. E. 2007, ApJ, 668, 1232
Fisher, G. H., Bercik, D. J., Welsch, B. T., & Hudson, H. S. 2012, SoPh, 277, 59
Fong, B., Low, B. C., & Fan, Y. 2002, ApJ, 571, 987
Gibson, S. E., & Fan, Y. 2006, ApJL, 637, L65
Gosain, S. 2012, ApJ, 749, 85
Hirayama, T. 1974, SoPh, 34, 323
Howard, R. A., Moses, J. D., Vourlidas, A., et al. 2008, SSRv, 136, 67
Hudson, H. S. 2000, ApJL, 531, L75
Hudson, H. S., Fisher, G. H., & Welsch, B. T. 2008, in ASP Conf. Ser. 383, Subsurface and Atmospheric Influences on Solar Activity, ed. R. Howe et al. (San Francisco, CA: ASP), 221
Jenkins, J. M., Long, D. M., van Driel-Gesztelyi, L., & Carlyle, J. 2018, SoPh, 293, 7
Jiang, C., Wu, S. T., Yurchyshyn, V., et al. 2016, ApJ, 828, 62
Kopp, R. A., & Pneuman, G. W. 1976, SoPh, 50, 85
Kushwaha, U., Joshi, B., Veronig, A. M., & Moon, Y.-J. 2015, ApJ, 807, 101
Liu, R., Liu, C., Török, T., Wang, Y., & Wang, H. 2012, ApJ, 757, 150
Liu, R., & Wang, H. 2009, ApJL, 703, L23
Liu, R., & Wang, H. 2010, ApJL, 714, L41
Pascoe, D. J., Russell, A. J. B., Anfinogentov, S. A., et al. 2017, A&A, 607, A8
Petrie, G. J. D. 2012, ApJ, 759, 50
Petrie, G. J. D. 2016, SoPh, 291, 791
Petrie, G. J. D., & Sudol, J. J. 2010, ApJ, 724, 1218
Rachmeler, L. A., DeForest, C. E., & Kankelborg, C. C. 2009, ApJ, 693, 1431
Russell, A. J. B., Simões, P. J. A., & Fletcher, L. 2015, A&A, 581, A8
Sarkar, A., Vaidya, B., Hazra, S., & Bhattacharyya, J. 2017, ApJ, 851, 120
Simões, P. J. A., Fletcher, L., Hudson, H. S., & Russell, A. J. B. 2013, ApJ, 777, 152
Sturrock, P. A. 1966, Natur, 211, 695
Sudol, J. J., & Harvey, J. W. 2005, ApJ, 635, 647
Sun, X., Bobra, M. G., Hoeksema, J. T., et al. 2015, ApJL, 804, L28
Sun, X., Hoeksema, J. T., Liu, Y., et al. 2012, ApJ, 748, 77
Sun, X., Hoeksema, J. T., Liu, Y., Kazachenko, M., & Chen, R. 2017, ApJ, 839, 67
Wang, H., & Liu, C. 2010, ApJL, 716, L195
Wang, J., Simões, P. J. A., Fletcher, L., et al. 2016, ApJ, 833, 221
Yan, X. L., Pan, G. M., Liu, J. H., et al. 2013, AJ, 145, 153
Zuccarello, F. P., Aulanier, G., Dudík, J., et al. 2017, ApJ, 837, 115
Zuccarello, F. P., Aulanier, G., & Gilchrist, S. A. 2015, ApJ, 814, 126